Dynamical Characteristics of Rydberg Electrons Released by a Weak Electric Field

Elias Diesen,[1] Ulf Saalmann,[1] Martin Richter,[2] Maksim Kunitski,[2] Reinhard Dörner,[2] and Jan M. Rost[1,3]

[1]*Max-Planck-Institut für Physik komplexer Systeme, Nöthnitzer Straße 38, 01187 Dresden, Germany*
[2]*Institut für Kernphysik, Goethe-Universität, Max-von-Laue-Straße 1, 60438 Frankfurt am Main, Germany*
[3]*PULSE Institute, Stanford University and SLAC National Accelerator Laboratory,*
2575 Sand Hill Road, Menlo Park, California 94025, USA

The dynamics of ultraslow electrons in the combined potential of an ionic core and a static electric field is discussed. With state-of-the-art detection it is possible to create such electrons through strong intense-field photoabsorption and to detect them via high-resolution time-of-flight spectroscopy despite their very low kinetic energy. The characteristic feature of their momentum spectrum, which emerges at the same position for different laser orientations, is derived and could be revealed experimentally with an energy resolution of the order of 1 meV.

Extracting excited electrons from an atom, molecule, or plasma with a constant electric field is an established technique that can reveal the minimal (Rydberg) excitation by tracking the electron yield as a function of applied field strength [1]. In the time domain, very small extraction fields of about $F = 1\ldots10$ V/cm (with 5.142 V/cm $= 10^{-9}$ a.u.) and high, pulsed Rydberg excitation lead to intricate electron dynamics despite the fact that a hydrogenic problem in an electric field is separable (e.g., in semi-parabolic coordinates), as we will demonstrate. Clearly, electrons that are capable to escape under such conditions must be highly excited and this is achieved in the experiment by a preceding excitation with a short intense laser pulse [2].

The kind of Stark dynamics discussed here with a focus on the differential momentum distribution of ionized electrons has not been investigated before, since ionization of Rydberg states in static or pulsed weak electric fields has mainly served the purpose to extract details of Rydberg states [zero-electron kinetic energy (ZEKE) spectroscopy] [1,3,4]. Individual classical trajectories and their contributions to the electron yield, on the other hand, have been investigated both in the context of astrophysics, where the same Stark Hamiltonian arises from a combined gravitational and constant driving field [5], and in an atomic setting. For the latter, the inclusion of phases to account for the interference effects of the different pathways to a detector [6–8] even lead beyond a classical treatment.

The results presented here are relevant for all experiments using electric-field extraction techniques, in particular the cold target recoil ion momentum spectroscopy (COLTRIMS) [9] technique, nowadays used routinely in reaction microscopes (REMIs) world wide. At very low energies, the Stark dynamics described here will modify the results expected in such setups. Moreover, it adds another interesting feature to the low-energy kinetic-energy spectrum of electrons ionized by an intense laser pulse, a process that has received a lot of attention [10–14] since the discovery of the so called low-energy structure [15,16].

Sufficient for our purpose, we will consider a hydrogenic problem governed by the Hamiltonian (atomic units are used unless stated otherwise)

$$\mathcal{H} = \mathsf{H} + \mathbf{r} \cdot \mathbf{f}(\mathsf{t}) \cos \omega \mathsf{t} \qquad (1)$$

with the Stark Hamiltonian

$$\mathsf{H} = \frac{\mathbf{p}^2}{2} - \frac{Q}{\mathsf{r}} - F\mathsf{z}, \quad \mathsf{r} = \sqrt{\mathsf{x}^2 + \mathsf{y}^2 + \mathsf{z}^2}, \qquad (2)$$

ionic charge $Q = 1$ (which could assume any, also non-integer, value) and a constant electric field of strength F pointing in the negative z direction. The second term in Eq. (1) describes the interaction with the laser pulse of (a strong but otherwise arbitrary) envelope $\mathbf{f}(\mathsf{t})$, linearly polarized along or perpendicular to the direction of the extraction field along the z direction in H. This combination of fields leads to the "zero-energy" structure observed in the strong field photoionization spectrum with REMIs [17]. However, the strong laser pulse only serves to populate the Rydberg states that form the initial condition for the unusual Stark dynamics we are going to discuss. Any other means to create the Rydberg population would lead to the same result if the Rydberg atoms are placed in a tiny electric field of the order of 10 V/cm: the photoelectron spectrum exhibits a peak not at zero energy but slightly upwards at a field-corrected photoelectron momentum [defined in Eq. (3) below] of $\boldsymbol{\pi}^* = -0.6F^{1/4}$, with the asterisk indicating the peak value.

Assuming $\ell_z = 0$ we eliminate the dynamics in the cyclic azimuthal angle. This reduction is possible as the laser-induced dynamics occurs on a length scale (given by the quiver amplitude, typically a few nanometers), which is much smaller than the barrier distance (typically a micron)

of the Stark Hamiltonian (2), and confirmed by the excellent agreement with full 3D simulations. Since the momentum of the electron increases under $\mathcal{H}$ as $\mathbf{p}_z \propto \sqrt{z}$ or $\mathbf{p}_z \propto t$, with distance z from the nucleus or time t, respectively, its value depends on where it is measured. To avoid such a dependence, the experimental time of flight t_{of} is used to construct an effective momentum

$$\boldsymbol{\pi} \equiv \mathbf{p}_z(t_{of}) - Ft_{of}, \qquad (3)$$

which eliminates the effect of the constant electric field asymptotically [18]. Consequently, Π does not depend on the position of the detector if placed sufficiently far beyond the barrier. This is a convenient procedure since experimentally the time of flight t_{of} and the detector distance z_d are known. Equivalent to Eq. (3), one obtains $\boldsymbol{\pi} = z_d/t_{of} - Ft_{of}/2$. Hence, a time delay—due to the retarded motion across the saddle point in the Stark geometry—is measured via t_{of}. Nevertheless, in experimental studies using REMIs $\boldsymbol{\pi}$ is referred to simply as the momentum component $\mathbf{p}_z$ of the electron parallel to the field direction of the spectrometer [9] tacitly assuming that the electron motion can be split between an interaction region, where the extraction field can be neglected, and an asymptotic region, into which the electron is launched with initial momentum $\mathbf{p}_z$. It is this separation that breaks down for the situation discussed here.

In Fig. 1 we compare classical simulation according to $\mathcal{H}$ given in Eq. (1) with experimental results [17] obtained for

argon atoms in a strong few-cycle pulse with $\lambda = 3200$ nm. Those experiments were the first to report a "zero peak," i.e., an extremely narrow contribution of near-zero momentum electrons [17], subsequently confirmed and attributed to Rydberg electrons [19]. We use standard tunnel-ionization probabilities [10,20] and propagate electrons according to the Newton equations of motion for about 10^7 trajectories with the Hamiltonian (1), i.e., in the attractive Coulomb potential, the driving laser pulse $\mathbf{f}(t) \cos \omega t$, and the extraction field F. Hence, the calculations comprise the formation of Rydberg electrons [2] as well the subsequent Stark dynamics. The experimental results [17] shown in Figs. 1(b)–1(d) are symmetrized in $\boldsymbol{\pi}$ with respect to $\boldsymbol{\pi} = 0$ and show a double peak very close to $\boldsymbol{\pi} = 0$. As one can see, the likewise symmetrized classical spectra agree extremely well with the experiment. However, a careful inspection of Fig. 1(a) reveals that the Rydberg peak is asymmetric with position $\boldsymbol{\pi}^* < 0$, pointing into the opposite direction of the extraction field F, i.e., parallel to the actual electric field.

With a setup where the laser polarization is along the y axis, i.e., perpendicular to the extraction field along z, we can prove that the peak and its negative offset in $\boldsymbol{\pi}$ is exclusively due to the extraction field F, see Fig. 2. Both the calculation and the experiment reveal the peak close to zero and again with a negative shift in the static field direction, here $\boldsymbol{\pi}_\perp$. We also note the qualitative agreement between theory (for argon atoms) and experiment (for N_2 molecules), which demonstrates that the laser pulse only prepares the initial Rydberg distribution for the ensuing
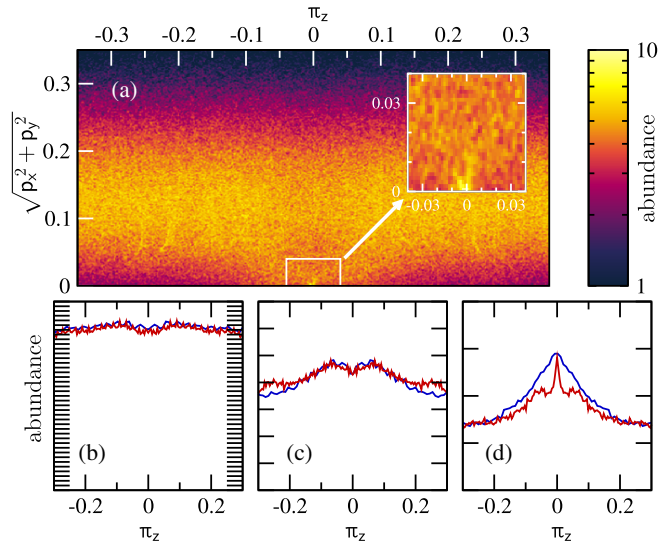

FIG. 1.   (a) 2D momentum map of photoelectrons from Ar atoms ionized with a laser pulse $\mathbf{f}(t) = \mathbf{e}_z f(t/T) \cos(\omega t)$ with $T = 64$ fs and $\omega = 0.3875$ eV ($\lambda = 3.2$ μm) and an extraction field $F = 1.5$ V/cm along the z axis. Lower panels: spectra as obtained by integrating the 2D distributions over (b) $\mathbf{p}_\perp = 0 \ldots 0.35$, (c) $\mathbf{p}_\perp = 0.02 \ldots 0.06$, and (d) $\mathbf{p}_\perp = 0.0 \ldots 0.02$, respectively. Calculations (red lines) are compared to experimental data (blue, Ref. [17]). Note that these spectra are symmetrized with respect to $\boldsymbol{\pi}_\parallel$.
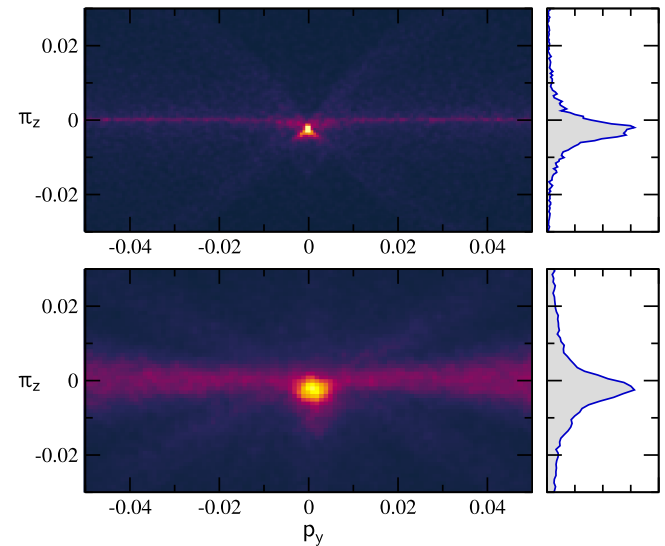

FIG. 2.   Momentum distribution of photoelectrons with $|p_x| < 0.01$, whereby the extraction field (2.6 V/cm) is perpendicular to the polarization of the laser pulse (780 nm), i.e., $\mathbf{f} \perp \mathbf{e}_z$, which is in contrast to Figs. 1 and 3(b). Upper panel: calculation for Ar. Lower panel: measurement for N_2. Each panel shows the 2D distribution and the one integrated over the parallel momentum in the interval $|p_y| < 0.005$.

Stark-field dynamics. It takes place far away from the (ionic) core whose exact nature hardly matters.

Backed by these results we concentrate now on the Hamiltonian (2) classically. Scaled phase-space variables

$$\{x, y, z, r\} = F^{1/2}\{\mathsf{x}, \mathsf{y}, \mathsf{z}, \mathsf{r}\} \tag{4a}$$

$$\{p_x, p_y, p_z\} = F^{-1/4}\{\mathsf{p_x}, \mathsf{p_y}, \mathsf{p_z}\} \tag{4b}$$

and time $t = F^{3/4}\mathsf{t}$ eliminate the dependence on F in Eq. (2) with the new Hamiltonian

$$H = \frac{\boldsymbol{p}^2}{2} - \frac{1}{r} - z. \tag{5}$$

This has two advantages: first, the (experimental) dependence of certain observables on the field strength F can be immediately predicted, which applies to all momenta including $\boldsymbol{\pi} = F^{1/4}\pi$ with $\pi = p_z - t$; secondly, the numerical problem simplifies considerably to that of a single effective field strength ($F = 1$) with a reasonable (effectively an atomic-scale) range for the phase-space variables.

We immediately conclude that the offset of the peak position Π^* from zero should scale with $F^{1/4}$ as confirmed by our experiment, see Fig. 4. While the shift of the peak position with increasing extraction voltage or extraction field might have been expected, the very existence of a peak is not obvious on first glance since one would expect that the (almost homogeneously) distributed Rydberg population is set free by the extraction field in a certain interval $\Delta E \ldots 0$, with the lower bound ΔE given by the barrier formed by the static field. This should lead to a finite value of the photoelectron spectrum at zero momentum but not to a peak, even systematically shifted from zero.

To understand the peak and its position π^* we take a closer look at the classical dynamics of the Stark Hamiltonian (5). To this end we propagate trajectories starting at the origin $z = \tilde{\varrho} = 0$, with the "directed" distance $\tilde{\varrho} \equiv \pm\sqrt{x^2 + y^2}$ from the z axis. The sign is positive (negative) if the electron has passed the z axis an even (odd) number of times [21]. The initial distribution is uniform in energy E and angle $\cos\theta_{\text{init}}$ in accordance with the uniform occupation of the Rydberg states. It turns out that for $E < 0$ initial angles where $\cos(\theta_{\text{init}}) < E^2/2 - 1$ lead to bound trajectories, despite the fact that they have an energy above the barrier $E_b = -2$. These are the well-known bound states in the continuum [1], which are a consequence of the separability of the hydrogen problem in an electric field [5] and account for $1/3$ of all trajectories in the range $E = -2 \ldots 0$. The other $2/3$ of the trajectories will escape. The abundance of the resulting final momenta π and $\tilde{p}_\varrho$ for those free trajectories are shown as a contour plot in Fig. 3(a). The final momentum $\tilde{p}_\varrho = \pm\sqrt{p_x^2 + p_y^2}$
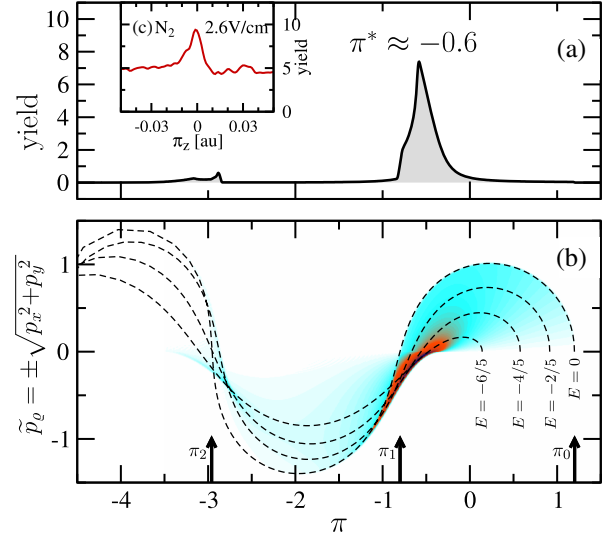

FIG. 3. Classical momentum spectra generated from a uniform population of energies $E = -2 \ldots 0$ and an isotropic distribution of $\cos\theta_{\text{init}}$. (a) Contour plot as a function of the scaled final momenta π and $\tilde{p}_\varrho$. The dashed lines show the final momenta for the four energies indicated in the graph and initial angles in the range $\theta_{\text{init}} = 0 \ldots \arccos(E^2/2 - 1)$. The arrows indicate the location of the zeros $\tilde{p}_\varrho(\pi_n) = 0$ for $E = 0$ according to Eq. (7). (b) The spectrum as a function of π after integration over the radial momentum $|\tilde{p}_\varrho| \leq 0.1$ (solid) and (c) the measured momentum for N_2 molecules ionized with a 780 nm pulse of 45 fs duration with the laser and extraction field parallel.

perpendicular to the extraction field oscillates as a function of π, with decreasing amplitude and period for each fixed energy E (dashed lines). Amplitudes also decrease at a fixed momentum $\tilde{p}_\varrho$ for decreasing energy E. This topology gives rise to a caustic of final momenta around $\{\pi^*, \tilde{p}_\varrho^*\} \approx \{-0.6, 0\}$. Indeed this caustic induces a divergent ridge, which becomes finite upon a finite resolution.

The peculiar structure of the momentum map in Fig. 3(a) becomes understandable when taking advantage of the separability of the Stark Hamiltonian in semiparabolic
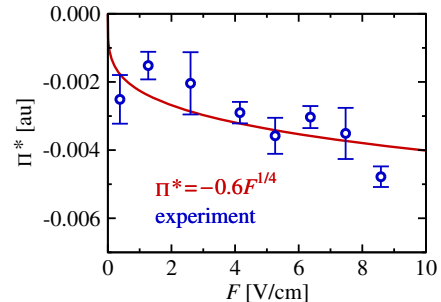

FIG. 4. Shifting of peak position Π^* with the extraction field strength F for photoionization of N_2, cf. Fig. 3(c). The experimental determination is described in the Supplemental Material [22]. Note that the prefactor in $\pi^* = -0.6F^{1/4}$ has been obtained theoretically from Fig. 3 and is not a fitting factor.

coordinates $\{u, v\} \equiv \{\sqrt{r+z}, \pm\sqrt{r-z}\}$. Here, the sign for v corresponds to the sign of $\tilde{\varrho}$. In these coordinates H from Eq. (5) assumes the form [22]

$$p_u{}^2/2 - Eu^2 - u^4/2 = 1 + \beta, \qquad (6a)$$

$$p_v{}^2/2 - Ev^2 + v^4/2 = 1 - \beta, \qquad (6b)$$

where β, the separation constant due to the additional dynamical symmetry, is fixed by the initial angle (in real space) according to $\beta = \cos\theta_{\text{init}}$ as shown in the Supplemental Material [22]. The separation (6) is connected with a new time τ, related to the real time t via $dt = (u^2 + v^2)d\tau$.

The separability allows one to understand the origin of the oscillating final electron momentum $\pi(\tilde{p}_\varrho)$ realizing that asymptotically for large z or u the Cartesian momenta are mapped as $\{p_z, \tilde{p}_\varrho\} \to \{u, v\}$ [22]. As can be seen from Eq. (6), the dynamics is that of a bound (v) and inverted (u) quartic oscillator at an energy $1 \mp \beta$. The partition of the effective energy between the two modes is controlled by β. For $\beta = 1$ or $\cos\theta_{\text{init}} = 0$ all energy is in u leading to the quickest possible escape with the largest value π for $u \to \infty$ while no energy is left for the bound oscillator, which stays at the fixed point $v = 0$. Decreasing β, keeping E fixed, reduces the effective energy in u and provides in turn some energy for oscillations in v. Once there is enough energy for the v oscillator to complete half an oscillation during escape, the electron will end up again at $v(\tau \to \tau_\infty) = 0$. Hereby, τ_∞ is the escape time in u, which is finite due to the quartic term in Eq. 6(a). Hence, we can define a series π_n, for which asymptotically $v = 0$ and therefore $\tilde{p}_\varrho = 0$, with $n = 0, 1, \ldots$ half oscillations in v. Despite the ever increasing momentum due to the acceleration from the electric field, the π_n are finite owing to the definition of $\pi = p_z - t$, cf. Eq. (3), which compensates exactly the acceleration.

Analytical quadratures for the quartic oscillator dynamics in the form of combinations of elliptic functions exist [5], but do not yield simple expressions describing the prominent features of Fig. 3. Yet, for the highest energy $E = 0$ these integrals simplify and permit us to determine the zeros of $\tilde{p}_\varrho(\pi)$ analytically

$$\pi_n = \pi|_{\tilde{p}_\varrho = 0} = \frac{2(1 - 2n^2)}{(1 + 4n^4)^{1/4}} \frac{\sqrt{\pi}\Gamma(3/4)}{\Gamma(1/4)}, \qquad (7)$$

see Ref. [22]. The arrows in Fig. 3(b) indicate the positions of the π_n according to Eq. (7) in good agreement with the numerical results.

While the π_n do not give the exact clustering positions they follow the same qualitative evolution and provide analytical insight for the latter: the second clustering near π_2 is much weaker because it takes place at smaller values of β as compared to π_1. For the zero crossings at $E = 0$ the corresponding values read $\beta_n = (1 - n^4)/(1 + n^4)$. Since

for escape, i.e., over-barrier motion, $E^2/2 < 1 + \beta$, the phase-space volume contributing to the caustics decreases with order n and the corresponding peak in the spectrum gets weaker.

We have verified with quantum calculations that quasibound states (resonances) cannot be responsible for the observed structure. This is plausible since the positions and widths of these resonances do not scale with F as classical calculations and experimental data do. Yet, the excellent agreement of our classical calculations with our experimental results raises the question why quantum effects do not play a role, in particular given the prominent presence of the potential barrier. The reason is the weakness of the field, which renders any action very large as can be directly inferred from the scaling (4). This applies to imaginary actions of tunneling paths and to real actions appearing as phases. Their differences scale with $F^{-1/4}$ and are large for small fields. Therefore, the interference between different trajectories is quenched leaving the classical limit as an excellent approximation.

In summary we have shown that the Stark dynamics of escaping Rydberg electrons leads to a peak in the spectrum of the effective momentum π or the time of flight as the experimental observable, changing its position with the field strength according to $\pi^*(F) = -0.6F^{1/4}$. This explains the occurrence of the "zero-energy structure" [17]. The universality of the phenomenon is underlined through the very good agreement with experiments where the initial Rydberg population was created by laser pulses of different wavelengths and for different targets (atoms and molecules). This peak is not only an unexpected and intricate consequence of the Stark dynamics; it also has direct implications for the experiment: the peak can be used to gauge the momentum scale if the field is known or vice versa, to determine the field strength with a known momentum scale.

[1] T. F. Gallagher, *Rydberg Atoms* (Cambridge University Press, Cambridge, England, 2005).
[2] T. Nubbemeyer, K. Gorling, A. Saenz, U. Eichmann, and W. Sandner, Phys. Rev. Lett. **101**, 233001 (2008).
[3] G. M. Lankhuijzen and L. D. Noordam, Phys. Rev. Lett. **76**, 1784 (1996).
[4] E. W. Schlag, *ZEKE Spectroscopy* (Cambridge University Press, Cambridge, England, 1998).
[5] G. Lantoine and R. P. Russell, Celest. Mech. Dyn. Astron. **109**, 333 (2011).
[6] V. D. Kondratovich and V. N. Ostrovsky, J. Phys. B **17**, 2011 (1984).
[7] Ch. Bordas, Phys. Rev. A **58**, 400 (1998).
[8] Ch. Bordas, F. Lépine, C. Nicole, and M. J. J. Vrakking, Phys. Rev. A **68**, 012709 (2003).

[9] J. Ullrich, R. Moshammer, A. Dorn, R. Dörner, L. Ph. H. Schmidt, and H. Schmidt-Böcking, Rep. Prog. Phys. **66,** 1463 (2003).

[10] A. Kästner, U. Saalmann, and J.-M. Rost, Phys. Rev. Lett. **108,** 033201 (2012); J. Phys. B **45,** 074011 (2012).

[11] C. Y. Wu, Y. D. Yang, Y. Q. Liu, Q. H. Gong, M. Y. Wu, X. Liu, X. L. Hao, W. D. Li, X. T. He, and J. Chen, Phys. Rev. Lett. **109,** 043001 (2012).

[12] L. Guo, S. S. Han, X. Liu, Y. Cheng, Z. Z. Xu, J. Fan, J. Chen, S. G. Chen, W. Becker, C. I. Blaga, A. D. Di Chiara, E. Sistrunk, P. Agostini, and L. F. Di Mauro, Phys. Rev. Lett. **110,** 013001 (2013).

[13] M. Möller, F. Meyer, A. M. Sayler, G. G. Paulus, M. F. Kling, B. E. Schmidt, W. Becker, and D. B. Milošević, Phys. Rev. A **90,** 023412 (2014).

[14] W. Becker, S. P. Goreslavski, D. B. Milošević, and G. G. Paulus, J. Phys. B **47,** 204022 (2014).

[15] C. I. Blaga, F. Catoire, P. Colosimo, G. G. Paulus, H. G. Muller, P. Agostini, and L. F. Di Mauro, Nat. Phys. **5,** 335 (2009).

[16] W. Quan, Z. Lin, M. Wu, H. Kang, H. Liu, X. Liu, J. Chen, J. Liu, X. T. He, S. G. Chen, H. Xiong, L. Guo, H. Xu, Y. Fu, Y. Cheng, and Z. Z. Xu, Phys. Rev. Lett. **103,** 093001 (2009).

[17] J. Dura, N. Camus, A. Thai, A. Britz, M. Hemmer, M. Baudisch, A. Senftleben, C. D. Schröter, J. Ullrich, R. Moshammer, and J. Biegert, Sci. Rep. **3,** 2675 (2013).

[18] In quantum mechanics, the momentum variable Π can be elegantly obtained directly through the interaction representation with $H_t = \mathcal{U} H \mathcal{U}^\dagger$ where $\mathcal{U} = \exp(-iFzt)$. Similarly, in classical mechanics, a canonical transformation with the generating function $\mathcal{F}_2 = (p_z + t)\bar{z}$ leads to new canonical variables $\bar{p}_z = \Pi$ and $\bar{z} = z$. In the velocity form of the Hamiltonian (2) π is the canonical momentum.

[19] B. Wolter, Ch. Lemell, M. Baudisch, M. G. Pullen, X.-M. Tong, M. Hemmer, A. Senftleben, C. D. Schröter, J. Ullrich, R. Moshammer, J. Biegert, and J. Burgdörfer, Phys. Rev. A **90,** 063424 (2014).

[20] N. I. Shvetsov-Shilovski, S. P. Goreslavski, S. V. Popruzhenko, and W. Becker, Laser Phys. **19,** 1550 (2009).

[21] Although motion is independent of the azimuthal angle, this angle jumps by 180° if the trajectory crosses the symmetry axis. This is reflected in the signs "±."

[22] See Supplemental Material at http://link.aps.org/supplemental/10.1103/PhysRevLett.116.143006, where the experimental determination of the peak positions is described and characteristics of the electron-momentum distribution are studied analytically.

Supplement for "Dynamical characteristics of Rydberg electrons released by a weak electric field"

Elias Diesen,[1] Ulf Saalmann,[1] Martin Richter,[2] Maksim Kunitski,[2] Reinhard Dörner,[2] and Jan M. Rost[1, 3]

[1]*Max-Planck-Institut für Physik komplexer Systeme, Nöthnitzer Straße 38, 01187 Dresden, Germany*
[2]*Institut für Kernphysik, Goethe-Universität, Max-von-Laue-Straße 1, 60438 Frankfurt am Main, Germany*
[3]*PULSE Institute, Stanford University and SLAC National Accelerator Laboratory,*
2575 Sand Hill Road, Menlo Park, California 94025, USA

We describe in detail how the time-of-flight (tof) corrected momentum peak Π^* is determined experimentally. Furthermore, we illustrate how to understand the oscillations in the electron momentum $\widetilde{p}_\varrho$, perpendicular to the electric field axis, as a function of π, the tof corrected momentum parallel to the axis. For $E = 0$ one can determine analytically the values π for which $\widetilde{p}_\varrho(\pi) = 0$.

A. Experimental determination of peak positions

Three aspects determine the accuracy of the measured peak position Π^*: (i) calibration of the detector, (ii) calibration accuracy of the origin $\pi_z = 0$, and (iii) statistical error due to inaccuracy in measurable quantities and experimental parameters (time-of-flight, distance from target to the detector, electric field). The calibration of the detector, corresponding to the stretch of the y-axis in Fig. 5 of the manuscript, is usually done by fitting the energy spacing between ATI-peaks, which is known to be equal to the photon energy (1.59 eV in our case). The accuracy of this procedure is about 5 %. The origin $\pi_z = 0$ was determined using the divergent momentum structure along $\pi_z = 0$ (see Fig. S1), which is a result of Coulomb focusing. Namely, the maxima of this structure were identified at up to six points along the p_y-axis by fitting perpendicular Gaussian distributions. The line connecting these maxima defines $\pi_z = 0$ as shown in Fig. S1.

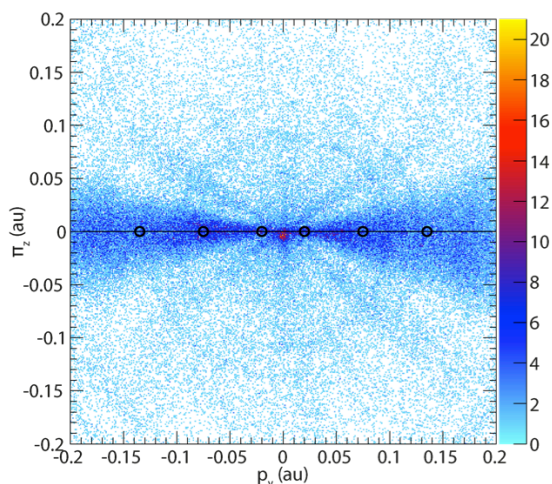The error bars in Fig. 5 correspond to inaccuracies in the determination of $\pi_z = 0$. The statistical error, i.e.,

FIG. S1: Measured photo-electron spectrum for N_2 for an extraction field of $F = 2.6$ V/cm. This corresponds to Fig. 2 of the main paper.

the standard deviation of $\pi_z(z_d, t_{\mathrm{of}}, F) = z_d/t_{\mathrm{of}} - F t_{\mathrm{of}}/2$ has been estimated using the variance formula

$$\Delta\pi_z = \sqrt{\left[\frac{\Delta z_d}{t_{\mathrm{of}}}\right]^2 + \left[\frac{\Delta F\, t_{\mathrm{of}}}{2}\right]^2 + \left\{\left[\frac{F}{2} + \frac{z}{t_{\mathrm{of}}{}^2}\right]\Delta t_{\mathrm{of}}\right\}^2}\,.$$

From the experimental parameters and their uncertainties $z_{\mathrm{det}} = 390$ mm, $\Delta z_{\mathrm{det}} = 50\,\mu$m (laser focus fluctuation), $F = 1\ldots 9$ V/cm, $\Delta F = 0.6\ldots 8.7 \times 10^{-3}$ V/cm, $t_{\mathrm{of}} = 70\ldots 260$ ns, $\Delta t_{\mathrm{of}} = 0.2$ ns, one gets a standard deviation of $3\ldots 14 \times 10^{-3}$ au. This uncertainty can also be deduced by comparing the experimentally measured peak with the theoretical one (Fig. 3 of the manuscript). The experimental peak is broader by about 5×10^{-3} au due to the statistical uncertainty. Despite of this relatively large uncertainty reflected in the peak width, the central position Π^* of the peak can be determined with much higher accuracy by fitting the peak to a Gaussian function.

B. Transformation to semi-parabolic coordinates

In contrast to Eq. (5) of the main paper, we use scaled cylindrical coordinates $\{\widetilde{\varrho}, z\}$ in which the Stark Hamiltonian reads

$$H = \frac{\widetilde{p}_\varrho{}^2}{2} + \frac{p_z{}^2}{2} - \frac{1}{r} - z, \quad r = \sqrt{\widetilde{\varrho}^2 + z^2}. \tag{1}$$

Here we have assumed $\ell_z = 0$ and thus ignore the dynamics in the cyclic azimuthal angle ϕ. As already discussed in the main paper, $\widetilde{\varrho}$ measures the "directed" distance from the symmetry axis. This allows in an intuitive way to account for crossings of this axis, which otherwise correspond to jumps of ϕ by $180°$.

The Hamiltonian H can be transformed into semi-parabolic coordinates $\{u, v\}$, with $s = \mathrm{sign}(\widetilde{\varrho}) = \pm 1$,

$$u = \sqrt{r+z}, \quad v = s\sqrt{r-z}, \tag{2a}$$

$$p_u = s\sqrt{r-z}\,\widetilde{p}_\varrho + \sqrt{r+z}\,p_z, \tag{2b}$$

$$p_v = \sqrt{r+z}\,\widetilde{p}_\varrho - s\sqrt{r-z}\,p_z, \tag{2c}$$

where it separates [1], cf. Eq. (6) in the main paper, into

$$E_u = \frac{p_u^2}{2} + V_u(u), \quad V_u(u) = -Eu^2 - \frac{u^4}{2} \tag{3a}$$

$$E_v = \frac{p_v^2}{2} + V_v(v), \quad V_v(v) = -Ev^2 + \frac{v^4}{2} \tag{3b}$$

with the condition $E_u + E_v = 2$ or using a separation constant β

$$E_u = 1 + \beta, \quad E_v = 1 - \beta. \tag{3c}$$

The $\{u, v\}$-motion described by Eqs. (3) has its own time τ, which is related to the original time t according to

$$dt = (u^2 + v^2) \, d\tau. \tag{4}$$

For completeness we also give the transformation back to the coordinates of the original Hamiltonian (1)

$$\widetilde{\varrho} = uv, \quad z = (u^2 - v^2)/2, \quad r = (u^2 + v^2)/2, \tag{5a}$$

$$\widetilde{p}_\varrho = \frac{up_v + vp_u}{u^2 + v^2}, \quad p_z = \frac{up_u - vp_v}{u^2 + v^2}, \tag{5b}$$

which will be used below.

C. Trajectories

We are interested in trajectories starting at the Coulomb singularity $\widetilde{\varrho}_{\text{init}} = z_{\text{init}} = 0$ or equivalently at the origin $u_{\text{init}} = v_{\text{init}} = 0$. Each trajectory is characterized by its energy E and the initial angle $\theta_{\text{init}} = \arctan\left(p_z^{\text{init}}, \widetilde{p}_\varrho^{\text{init}}\right)$. In the separated system (3) the trajectories are characterized by the energy E, which is now a parameter in the potentials, and the separation constant $-1 \le \beta \le 1$, which is related to the initial angle

$$\beta = \cos\theta_{\text{init}}. \tag{6}$$

The initial momenta can be written as $p_u^{\text{init}} = 2\cos(\theta_{\text{init}}/2)$ and $p_v^{\text{init}} = 2\sin(\theta_{\text{init}}/2)$.

The electron can escape if it has sufficient energy to pass the barrier of height $V_u(u_{\text{b}}) = E^2/2$ in u at $u_{\text{b}} = \sqrt{-E}$. From $E_u \le 2$ one sees that this requires at least $E \ge -2$. However, not all trajectories which fulfil this condition escape. Rather, the angle θ_{init} must be such, that there is sufficient energy in the u-degree of freedom, which implies $E_u > E^2/2$ or

$$\cos\theta_{\text{init}} > E^2/2 - 1, \tag{7}$$

which follows from Eqs. (3c) and (6). Hence, one can calculate the fraction of electrons which escape over the Stark barrier

$$\eta = \frac{I\left(\arccos(E^2/2 - 1)\right)}{I(\pi)} \tag{8a}$$

$$I(x) \equiv \int_{-2}^0 dE \int_0^x d\theta_{\text{init}} \, \sin\theta_{\text{init}} \tag{8b}$$

to get $\eta = 2/3$. In Eqs. (8) we have assumed that the energies E and $\cos\theta_{\text{init}}$ are uniformly distributed.

D. Asymptotic momenta

1. General

For an escaped trajectory ($u \to \infty$) $p_u{}^2 \to u^4$ holds, as can be seen from (3a). Then,

$$\{\widetilde{p}_\varrho, p_z\} \stackrel{u \to \infty}{\longrightarrow} \{v, u\}, \tag{9a}$$

$$\pi = p_z - t \stackrel{u \to \infty}{\longrightarrow} u - t \tag{9b}$$

follows from Eq. (5b). Here, π is the effective momentum accounting for the time of flight as introduced in the main paper.

Due to the quartic term in (3a) the electron reaches $u \to \infty$ within a finite time which we call τ_∞,

$$\tau_\infty = \int_0^{\tau_\infty} d\tau = \int_0^\infty \frac{du}{\dot{u}}, \quad \dot{u} = du/d\tau. \tag{10}$$

Note, that the corresponding real time t, which follows from integrating Eq. (4),

$$t_{\text{fin}} = \int_0^{t_{\text{fin}}} dt = \int_0^{\tau_\infty} d\tau \, (u^2 + v^2), \tag{11}$$

is infinite.

The time-evolution in v is periodic. Hence, the time, it takes to reach $v_{\text{fin}} = v(\tau_\infty)$ in the end, is the number n of half-periods T plus the final stretch v_{fin},

$$\tau_{n,v_{\text{fin}}} = \int_0^{\tau_{n,v_{\text{fin}}}} d\tau = nT + \int_0^{v_{\text{fin}}} \frac{dv}{\dot{v}} \tag{12a}$$

$$T = 2 \int_0^{v_{\text{tp}}} \frac{dv}{\dot{v}}, \quad \dot{v} = dv/d\tau, \tag{12b}$$

where v_{tp} is the turning point of the potential V_v in Eq. (3b).

Since asymptotically $v = \widetilde{p}_\varrho$, cf. Eq. (9a), one can fix a certain asymptotic momentum $\widetilde{p}_\varrho$ by defining v_{fin}. Setting $\tau_\infty = \tau_{n,v_{\text{fin}}}$ gives multiple solutions for which trajectories characterized by $\{\beta_n, E_n\}$ lead to a particular v_{fin} and thus to an asymptotic momentum $\widetilde{p}_\varrho$.

For asymptotic large times at the detector only the difference $\pi \equiv p_z - t_{\text{fin}}$ will be finite, while t_{fin} and p_z will diverge. One can rewrite Eq. (11) as

$$t_{\text{fin}} = \int_0^\infty du \frac{u^2}{\dot{u}} + \int_0^{v_{\text{fin}}} dv \frac{v^2}{\dot{v}}. \tag{13}$$

From (9b) one gets with (13) an explicit expression for the effective momentum at time t_{fin}

$$\pi = \int_0^\infty du \left(1 - \frac{u^2}{\dot{u}}\right) - \int_0^{v_{\text{fin}}} dv \frac{v^2}{\dot{v}}. \tag{14}$$

This fixes the zeros of $\widetilde{p}_\varrho(\pi) = 0$, i.e., those pairs of $\{E, \theta_{\text{init}}\}$ for which $\widetilde{p}_\varrho$ vanishes.

2. Special case $E = 0$

For trajectories with $E = 0$ these zeros can be obtained analytically. For τ_∞ we get with Eqs. (3a) and (10)

$$\tau_\infty^{E=0} = (2 + 2\beta)^{-1/4} \int_0^\infty \frac{du}{\sqrt{1 + u^4}}$$
$$= \frac{\left[2\Gamma(\frac{5}{4})\right]^2}{[2 + 2\beta]^{1/4}\sqrt{\pi}} \tag{15}$$

For the half period (12b) in v we have with $v_{\text{tp}} = 1$ in scaled coordinates

$$T^{E=0} = 2[2 - 2\beta]^{-1/4} \int_0^1 \frac{dv}{\sqrt{1 - v^4}}$$
$$= \frac{2\sqrt{\pi}\Gamma(\frac{5}{4})}{[2 - 2\beta]^{1/4}\Gamma(\frac{3}{4})}. \tag{16}$$

The condition $\tau_\infty = \tau_{n,0} = n\,T$ picks trajectories which end after n half periods right at $v = 0$ or equivalently $\widetilde{p}_\varrho = 0$, which is what we are looking for. The corresponding values for β follow from Eqs. (15) and (16)

$$\frac{1 - \beta_n}{1 + \beta_n} = n^4 \left[\frac{\pi}{2} \frac{1}{\Gamma(\frac{5}{4})\Gamma(\frac{3}{4})}\right]^4 = 4n^4. \tag{17}$$

We can now calculate Eq. (14) for $E = 0$ similarly as in (15) and (16) using (17). For the case $E = 0$, it assumes the simple form

$$\pi_n = (2 + 2\beta)^{1/4}\pi_u - 2n(2 - 2\beta)^{1/4}\pi_v, \tag{18a}$$
$$\pi_v \equiv \frac{\sqrt{\pi}\Gamma(\frac{3}{4})}{\Gamma(\frac{1}{4})}, \quad \pi_u \equiv \sqrt{2}\pi_v. \tag{18b}$$

Hence, finally the effective momenta for which $E = 0$ and $\widetilde{p}_\varrho = 0$ are given as

$$\pi_n = \frac{2(1 - 2n^2)}{(1 + 4n^4)^{1/4}}\pi_v \tag{19}$$

For large n the the corresponding momenta π_n decrease linearly with n, $\pi_{n\to\infty} = -2\sqrt{2}n\pi_v$. The first few values are $\pi_0 = 1.2$, $\pi_1 = -0.80$, $\pi_2 = -2.95$, $\pi_3 = -4.80$, where π_1 is structurally related to the main caustic producing the peak in the spectrum while π_2 is correspondingly related to the second, weaker caustic.

[1] G. Lantoine and R. P. Russell, Celest. Mech. Dyn. Astron. **109**, 333 (2011).